On the geometry of plastic potential surfaces and isochoric stress paths

Sur la géométrie des surfaces potentielles plastiques et des chemins de contraintes isochores

Biru Tsegaye A., Benz T.,Nordal S.
Norwegian university of Science and Technology (NTNU)

ABSTRACT: In this paper, isochoric stress paths are studied considering an elastic perfectly plastic model and a simple hardening plasticity model. Both associated and non-associated flow rules are considered. The effect of geometry of plastic potential functions on the evolution of stress paths is illustrated. Plastic potential functions of the Mohr-Coulomb type and the Drucker-Prager type are considered. Finally, relevant conclusions are given.

RÉSUMÉ : Dans cet article, des chemins de contraintes isochores sont étudiés, en considérant deux modèles: un modèle élastique parfaitement plastique, et un modèle à simple durcissement plastique. Les lois d'écoulement, tant associées que non-associées, sont considérées. L'effet de la géométrie des fonctions potentielles plastiques, sur l'évolution des chemins de contraintes, a été illustré. Les fonctions potentielles plastiques de types Mohr-Coulomb et Drucker-Prager sont considérées. Enfin, des conclusions sont données sur l'ensemble de ces sujets.

KEYWORDS: geometric non-coaxiality, deviatoric non-associativity, deviatoric plane plots,

1 INTRODUCTION

Several soil models of varying degree of complexity, many of them within the elastoplastic framework, have been developed. Often, limited types of deformation modes are plotted for illustration of model responses. In this paper, two simple elastoplastic models are considered and various isochoric stress paths are plotted in a deviatoric plane such that the mobilization of different stress paths relative to the strain increment direction is investigated.

The mobilization of stress relative to (plastic) strain increment is studied in non-coaxiality theories. Findings indicate that (*e.g.*, Roscoe 1970, Thornton and Zhang 2006, Arthur *et al.* 1986):

- non-coaxiality vanishes with plastic shear strain although contradicting reports exist during post bifurcation deformation states (*e.g.*, Vardoulakis and Georgopoulos 2004, Gutierrez and Vardoulakis 2007).
- for an isotropic state, plastic strain increments and stress paths show reasonable coaxiality.

Similar observations can be inferred from a limited number of true triaxial tests in literature. For example, for isotropic state and proportional loading, the tests by Yamada and Ishihara (1981), and Jafarzadeh *et al.* (2008) show that

- at lower mobilizations, for radial proportional loading in a deviatoric plane, stress paths are also radial. At higher mobilization strain increment vectors show some deviation from the radial direction but are reasonably close (see for example, Figure 1).
- the total strain rate direction and the plastic strain rate directions are nearly the same.
- stresses and strain increments are hence reasonably coaxial.

Note: In the following sections stresses and friction angles are effective.

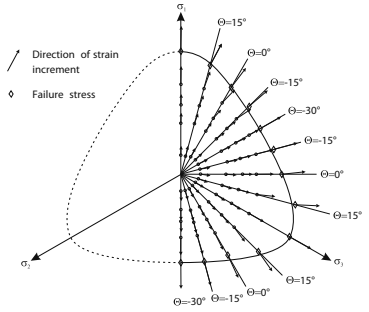

Figure 1: Deviatoric plots of effective stress path and orientation of plastic deviatoric strain increment (according to Yamada and Ishihara 1979).

2 ELASTO PLASTIC FRAMEWORK

Generally, in plasticity theory strain rate is additively decomposed into elastic and plastic such that the stress increment and the strain increment are related as

$$\dot{\boldsymbol{\sigma}} = \mathbf{C}^{ep}\dot{\boldsymbol{\varepsilon}}, \qquad (1)$$

where $\mathbf{C}^{ep}$ is the elastoplastic tangent stiffness tensor and may be decomposed as

$$\mathbf{C}^{ep} = \mathbf{C}^{e} + \mathbf{C}^{p}, \qquad (2)$$

where $\mathbf{C}^{e}$ is the elastic stiffness tensor and $\mathbf{C}^{p}$ is the stiffness degradation due to plasticity.

Furthermore, it is assumed that a stress state obeys a certain (yield) function and plastic strains are oriented normal to a plastic potential function. The plastic flow is distinguished associated if the potential function is the same as the yield function. Elastoplastic constitutive models for soil usually consider plastic potential functions different from the yield function. The plastic flow rule is then called non-associated flow rule. As will be shown in the following, geometric properties of the various surfaces affect the response of these models.

3 ELASTIC PERFECTLY PLASTIC MODEL WITH MOHR-COULOMB YIELD FUNCTION

Elastic-perfectly plastic abstractions are relatively simple and despite their shortcomings very popular. The main derive for their popularity is perhaps their similarity with limit equilibrium and linear elastic solutions and simple abstractions. However, some aspects of these models are still unexplored and overlooked.

In this section, a linear elastic perfectly plastic Mohr-Coulomb model with a linear elastic stiffness tensor following Hoek's law

$$C^e_{ijkl} = 2G\left[I^{sym}_{ijkl} + \frac{\nu}{1-2\nu}\delta_{ij}\delta_{kl}\right] \qquad (3)$$

is considered; where the shear modulus G and Poisson's ratio, ν, are elasticity parameters; and I^{sym}_{ijkl} is the so called Kronecker's delta.

The stiffness degradation due to plasticity, $\dot{\sigma}^p$, is established from the consistency condition in plasticity theory as

$$\dot{\sigma}^p = \frac{\partial^e : g_{,\sigma}\; \partial f_{,\sigma} : \dot{\varepsilon}^e}{f_{,\sigma} : \partial^e : g_{,\sigma}}, \qquad (4)$$

wherein f is the yield function and g is the plastic potential function, $x_{,\sigma} = \partial x / \partial \sigma$.

Here, the Mohr-Coulomb criterion is cast into a yield function. The Mohr-Coulomb criterion can be written in terms of stress invariants as

$$f = \sqrt{\frac{1}{2}s : s}\, A^R_K + \frac{3\sin\varphi_p}{3-\sin\varphi_p}\, p - a = 0, \qquad (5)$$

where $s = \sigma + \frac{1}{3}p\mathbf{1}$ is the deviatoric stress tensor and $p = \frac{1}{3}\sigma : \mathbf{1}$ is the mean normal stress. The peak friction angle, φ_p, is a model parameter and $a = c\cot\varphi_p$ is called attraction (Janbu 1973*a*), where c is cohesion.

The corresponding Mohr-Coulomb type plastic potential function may be written as

$$g = \sqrt{\frac{1}{2}s : s}\, A^R_{|Z|} + \frac{3\sin\psi_{max}}{3-\sin\psi_{max}}\, p, \qquad (6)$$

where maximum dilatancy angle, ψ_{max}, is additional model parameter.

The Lode angle dependent functions A^R_K and $A^R_{|Z|}$ can be found from trigonometric considerations in Figure 2 as

$$A^R_{K|Z} = \frac{\sqrt{3}\,\alpha_{K|Z}}{2\,\alpha_{K|Z}\sin\theta_1 + \sin\theta_2} \qquad (7)$$

where

$$\alpha_{K|Z} = \frac{3-\sin\varphi_{p,|\psi_{max}|}}{3+\sin\varphi_{p,|\psi_{max}|}} \qquad (8)$$

and

$$\theta_{1,2} = \frac{\pi}{6} \mp \theta_R. \qquad (9)$$

θ_R is the Lode angle defined here as

$$\theta_R = \frac{1}{3}\arcsin\left[\frac{3\sqrt{3}J_3}{2J_2^{3/2}}\right] \qquad (10)$$

where $J_3 = \det s$, $J_2 = \frac{1}{2}tr s^2$ (det = determinant, tr = trace).

For triaxial compression and extension deformation modes, the Lode angle, θ_R, is $\pi/6$ and $-\pi/6$ respectively.

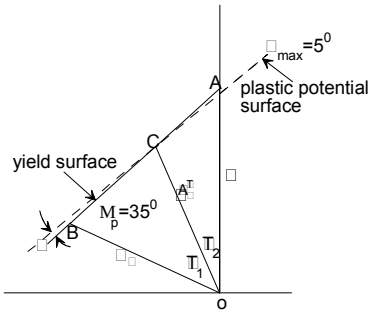

Figure 2: One sector of the Mohr-Coulomb surface (normalized by deviatoric stress at triaxial compression) in deviatoric plane in relation to a corresponding Mohr-Coulomb plastic potential function. A: Triaxial compression, B: Triaxial extension.

Stresses enclosed within the failure surface are elastic. On the failure surface, all strains are plastic. Generally, $\psi_{max} \neq \varphi_p$. When $\psi_{max} = \varphi_p$, associated flow rule is recovered and plastic strain increments are oriented normal to the failure surface given in Eq. (5).

It should be mentioned here that, although Eqs. (5) and (6) can be used for implementation of the model, in this study they are used for a short presentation only. The implementation is done by sorting eigenvalues of the stress tensor such that the Mohr-Coulomb criterion is established by choosing the major and the minor principal stresses.

In Figure 3, pure deviatoric strains, *i.e.*, isochoric condition, are applied and stress paths are plotted in the normalized deviatoric plane. The plots indicate that some stress paths deflect towards triaxial extension and compression modes. The less the maximum dilatancy angle the more is the deflection. At failure, the stress paths are therefore different from the principal strain rate increment directions, hence generally non-coaxial to the strain increment direction. This non-coaxiality is inherent to the geometry of the potential surface in the deviatoric plane and hence distinguished here as geometric non-coaxiality. Often, typical plots are illustrated for triaxial extension and compression states. However, the stress paths in between do not follow the trends of triaxial extension and compression stress paths as shown in Figure 3. Reasons are

- since the plastic potential function is a function of the major and the minor principal stresses, the intermediate stress state is not corrected for plasticity. Hence, touching the Mohr-Coulomb line does not guarantee that the stress state be a constant.
- the geometry of the potential surface causes a drift, since the normal to the surface is not necessarily coaxial to the current stress path.
- the drift may be amplified by deviatoric non-associativity.

Considering one of the six sectors in the normalized S-plane (Figure 2), two Mohr-Coulomb lines with friction angles φ_1 and φ_2 make an angle of

$$\beta = \arcsin\left[\frac{\sqrt{3}}{4}\,\frac{2\sqrt{4\sin^2\varphi_1 - 4\sin^2\varphi_2} - 2\sin\varphi_1\sqrt{4-4\sin^2\varphi_2}}{\sqrt{1-\sin^2\varphi_1\sin^2\varphi_2 - \sin\varphi_1\sin\varphi_2}}\right] \qquad (11)$$

with each other. This angle introduces deviatoric non-associativity when the yield function and the plastic potential function assume different angles, which is the case for non-associated flow. Deviatoric associativity may be achieved simply by considering $A^R_{|Z|}$. A^R

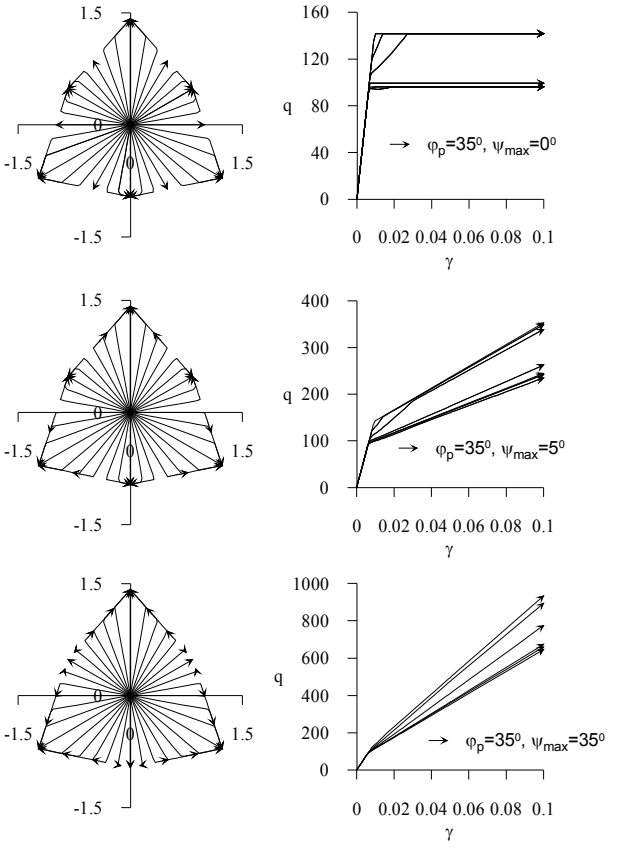

Figure 3: Plots of isochoric stress paths (for radial isochoric strain increments, a) in a deviatoric plane (normalized by mean normal stress) b) *p-q* plane and c) shear strain deviatoric stress plot, for an elastic perfectly plastic Mohr-Coulomb model with a Mohr-Coulomb plastic potential function. For all simulations G=5000kPa and v=0.3 are used.

This, however, will not fully solve the drift problem as illustrated in simulations using $\psi_{\max} = \varphi_p$, *i.e.*, associated plasticity (Figure 2).

4 SIMPLE ELASTIC PLASTIC HARDENING MOHR-COULOMB MODEL

To formulate a simple hardening model, the peak friction angle, φ_p, and the maximum dilatancy angle, $\psi_{\max}$, in Equations (5) and (6) are replaced by mobilized friction angle, φ_m, and mobilized dilatancy angle, ψ_m, respectively (see Figure 4). The increment of the sine of the mobilized friction angle is related to the plastic shear strain increment according to

$$d\sin\varphi_m = \tilde{G}^p \left(1-\tilde{\eta}_m\right)^2 d\gamma^p , \tag{12}$$

where $\tilde{G}^p = G^p / p$, $\tilde{\eta}_m = \sin\varphi_m / \sin\varphi_p$, G^p is a model parameter, called plastic shear modulus and $d\gamma^p$ is the plastic shear strain increment and here is defined as

$$d\gamma^p = \frac{3}{2} tr\dot{\mathbf{e}}^{p2} , \tag{13}$$

where $\dot{\mathbf{e}}^p = \dot{\boldsymbol{\varepsilon}}^p - \frac{1}{3}\dot{\boldsymbol{\varepsilon}}^p : \boldsymbol{\delta}$ is the plastic deviatoric strain rate tensor.

The plastic volumetric strain increment, $d\varepsilon_v^p = d\boldsymbol{\varepsilon}^p : \boldsymbol{\delta}$, is calculated as

$$d\varepsilon_v^p = \sin\psi_m d\gamma^p , \tag{14}$$

where $\sin\psi_m$ is the mobilized dilatancy angle.

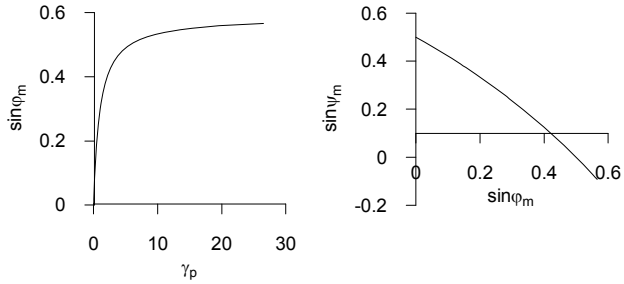

Figure 4: a) Hardening rule: mobilization of the sine of friction angle with plastic shear strains b) Plot of mobilized dilatancy angle with mobilized friction angle according to Rowe's stress-dilatancy rule.

The mobilized dilatancy angle is calculated from Rowe's stress-dilatancy relationship, which in assuming sign convention of soil mechanics, is given by

$$\sin\psi_m = -\frac{\sin\varphi_m - \sin\varphi_c}{1+\sin\varphi_m \sin\varphi_c} , \tag{15}$$

where φ_c is the critical state friction angle.

Consequently, the stiffness degradation due to plasticity is given by

$$\mathbf{C}^p = -\frac{\mathbf{C}^e : g_{,\boldsymbol{\sigma}} \otimes f_{,\boldsymbol{\sigma}} : \mathbf{C}^e}{f_{,\boldsymbol{\sigma}} : \mathbf{C}^e : g_{,\boldsymbol{\sigma}} - H} . \tag{16}$$

The term, H, added here is called hardening modulus and is obtained as

$$H = \frac{2}{3}\tilde{G}^p \left(1-\tilde{\eta}_m\right)^2 d\gamma^p f_{,\sin\varphi_m} : g_{,\boldsymbol{\sigma}} , \tag{17}$$

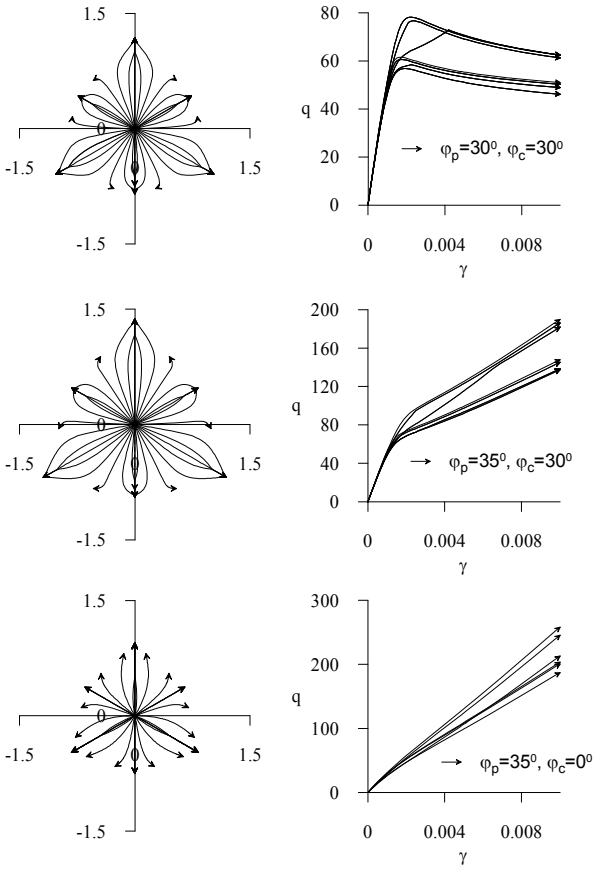

Figure 5: Effective stress path plots for radial isochoric strain increments, a) deviatoric plane (normalized by mean normal stress), b) *p-q* plane, c) deviatoric strain-deviatoric stress, for elastic plastic Mohr-Coulomb model with Mohr-Coulomb plastic potential function. For all simulations G=30000, G^p=30000 and v=0.3 are used.

where $f_{,\sin\varphi_m} = \partial f / \partial \sin\varphi_m$. When $\tilde{\eta}_m = 1$, Equations (4) and (16) are identical which means that all strains are then plastic.

As shown in Figure 5 the isochoric stress paths now start drifting early towards triaxial extension and compression modes. As plasticity starts early on, the drift is severe in the case of this simple hardening model. A drift of such an extent is not observed experimentally.

Associated flow rule can be retrieved by putting $\varphi_c = 0^0$ such that $\psi_m = \varphi_m$. The plots shown in Figure 5 demonstrate that associated flow rule is not a solution to the drift problem. Moreover, isochoric effective stress paths in the *p-q* plane are highly unrealistic.

5 RADIAL MAPPING AND A POSSIBLE GENERALIZATION

Radial mapping has been used by a number of authors (*e.g.*, Benz 2007, Tsegaye[1] 2010, Tsegaye *et al.* 2012). The implication of radial mapping is next investigated for the elastoplastic models considered in sections 3 and 4.

5.1 Isotropy and radial mapping

As shown herein before, Mohr-Coulomb type plastic potential function introduces unrealistic drift in stress path for radial strain increments. For an initially isotropic state, such a drift is not supported by experiments. True triaxial tests show that for an initially isotropic state and proportional loading, stress paths are nearly radial. Hence, radial mapping may be a reasonable assumption. Radial mapping can be interpreted that plastic strains orient themselves towards isotropic stress state (*i.e.*, radial to the hydrostatic axis). Coaxiality is maintained between principal strain increments and principal stresses for radially proportional loading paths.

Radial mapping can be easily achieved by considering Lode angle independent potential functions. For pressure sensitive materials like soils a function of the Drucker-Prager type, ensures radial return.

In Figure 6, responses of an elastic perfectly plastic model with a Mohr-Coulomb yield function and Drucker-Prager plastic potential function are plotted. As shown in the plots, isotropic radial strain increments produce radial stress paths. There is no deviatoric drift. The strength variation in between triaxial extension and compression is captured. Notice, however, the minimum strength is not due to triaxial extension but an in-between state that is located at the shortest distance from the hydrostatic axis. Figure 7 illustrates response of the simple hardening model with a Drucker-Prager plastic potential function to isochoric radial strain increments. The response in the deviatoric plane remains radial and the plots in *p-q* plane and *γ-q* plane are smooth.

5.2 Anisotropy and radial mapping

Anisotropy can be due to fabric constraint and/or induced by loading history, for example during deposition. It is important to remark here that if a generalization is to be made, at this stage it rests on very limited experimental data. For example considering the tests by Jafarzadeh *et al.* (2008), if each test was performed on a sample prepared at a different initial void ratio, stress path contours at constant deviatoric strain may not give a correct picture of the deviatoric response contours.

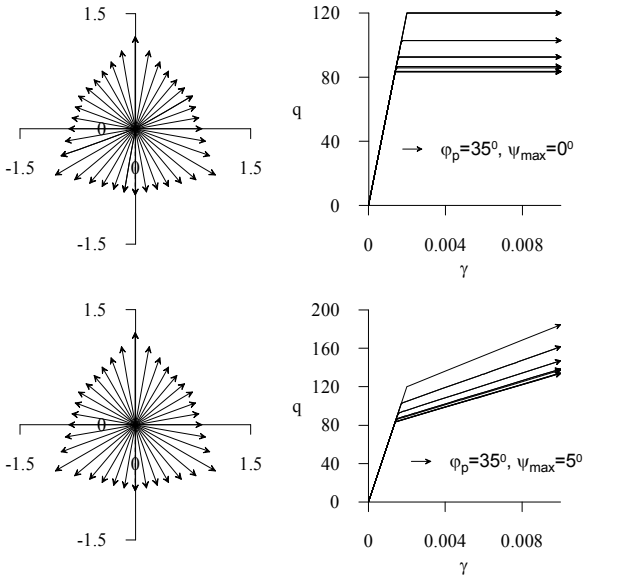

Figure 6: Plots of isochoric stress paths (for radial isochoric strain increments, a) in a deviatoric plane (normalized by mean normal stress) b) *p-q* plane and c) shear strain deviatoric stress plot, for an elastic perfectly plastic Mohr-Coulomb model with a Drucker-Prager plastic potential function. For all simulations G=5000kPa and v=0.3 are used.

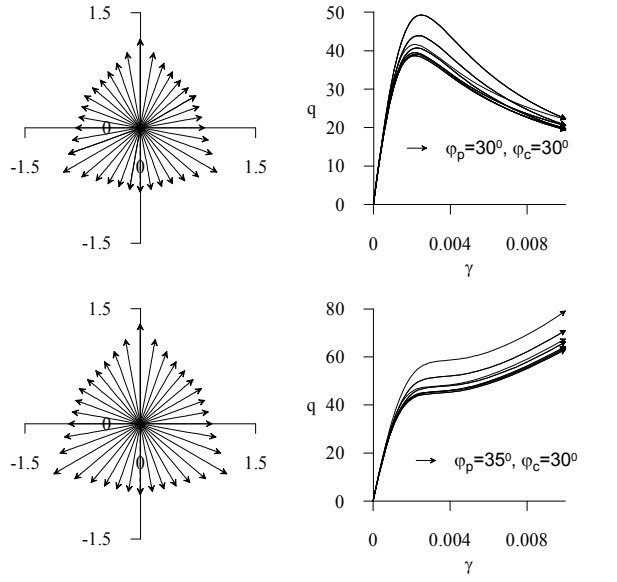

Figure 7: Effective stress path plots for radial isochoric strain increments, a) deviatoric plane (normalized by mean normal stress), b) *p-q* plane, c) deviatoric strain-deviatoric stress, for an elastic plastic Mohr-Coulomb model with Drucker-Prager plastic potential function. For all simulations G=30000 kPa, G^p=30000 kPa and v=0.3 are used.

Aside from that, the following observations could be noted.

- Initial anisotropy fades away during plastic deformation
- At larger mobilizations the critical state surface is not significantly affected by anisotropy.

The use of radial mapping for anisotropic initial stress state yields

- non-coaxial principal stress and principal strain increments. Since the direction of plastic strains is known a priori, the degree of non-coaxiality can be calculated as a state variable.
- fading memory of anisotropy and non-coaxiality with plastic distortion.

[1] Previous papers by the first author are published under the last name Tsegaye.

A more general approach may be devised by establishing a focal point for the direction of plastic strain increments. For example, if the center of the Drucker-Prager surface is shifted due to anisotropy, an evolution rule can be established such that the anisotropic center moves towards the hydrostatic axis as plastic deviatoric strains accumulate.

6 CONCLUSION

Due to advances in finite element packages, many soil models are implemented in general stress-strain space. Often however limited stress-strain paths are plotted to demonstrate model responses. In this paper, considering two simple models, stress paths are plotted in the deviatoric plane. When a Mohr-Coulomb type plastic potential function is implemented, unrealistic drift of stress paths towards triaxial extension and compression states is observed. The drift may be corrected by using radial mapping in the deviatoric plane. The possible consequence of radial mapping during anisotropic initial stress state is discussed.

7 REFERENCE

Arthur J.R.F., Koenders, M.A. & Wong, R.K.S. 1986. Anisotropy in particle contacts associated with shearing in granular media. *Acta mechanica* 64 (1-2), 19-29.

Benz, T.: Small-strain stiffness and its numerical consequences. PhD Thesis. Stuttgart University. Germany (2007).

Roscoe, K.H. 1970. The influence of strains in soil mechanics. *Géotechnique* 20 (2), 129-170.

De Josselin De Jong, G. 1976. Rowe's stress-dilatancy equation based on friction. *Géotechnique* 26 (3), 527-534.

Gutierrez, M. and Wang J. 2009. Non-coaxial version of Rowe's stress-dilatancy relation. *Granular Matter* 11 (2), 129-137.

Gutierrez M., Ishihara K. Non-coaxiality and energy dissipation in granular materials. Soils and Foundations 2000; 40 (2):49–59..

Jafarzadeh, F, Javaheri, H, Sadek, T. and Muir, Wood. D, 2008. Simulation of anisotropic deviatoric response of Hostun sand in true triaxial tests. *Computers and Geotechnics* 35 (6), 703-718.

Janbu N. 1973*a*. Shear strength and stability of soils, the applicability of the Colombian material 200 years after the ESSAI, in *Norsk geoteknisk forening*. Oslo: Norwegian Geotechniccal Institute, 1-47.

Pande G.N, Pietruszczak S. 1986. Symmetric tangential stiffness formulation for non-associated plasticity. *Computers and Geotechnics* 2, 89-99.

Rowe P.W. 1962. Stress-dilatancy relation for static equilibrium of an assembly of particles in contact. *Proc. R. Soc.* A-269:500-527.

Taylor, D.W. (1948). Fundamentals of soil mechanics. New York: J.Wiley and Sons.

Thornton C. and Zhang, L. 2006. A numerical examination of shear banding and simple shear non-coaxial flow rules. *Phi. Mag* **86**, N0. 21-22, 3425-3452.

Tsegaye, A.B. 2010. Plaxis liquefaction model. Report No.1 Plaxis, b.v., Delft, the Netherlands.

Tsegaye, A.B., Brinkgreve, R. Bonnier, R. Galavi, V. Benz, T. 2012. A simple effective stress model for sands-multiaxial formulation and evaluation. *Sec. Int. Conf. on Performance -Based Design in Earthquake Geotechnical Engineering*.

Tsegaye, A.B., Nordal S. and Benz T. 2012. On shear volume coupling of soils. *2nd Int. Symp. On Constitutive Modeling of Geomaterials.*

Yamada, Y. and Ishihara, K. 1979. Anisotropic deformation characteristics of sand under three dimensional stress conditions. *Soils and Foundations*, 19(1), 97-107.